Coupled-reaction-channel calculations of the $^{16}O+^{17}O$ and $^{16}O+^{17}F$ charge-symmetric systems

J.-M. Sparenberg and D. Baye
Université Libre de Bruxelles, Physique Nucléaire Théorique et Physique Mathématique, CP 229, Campus de la Plaine, B-1050 Bruxelles, Belgium

B. Imanishi
Ohto 1-3-1, Yono, Saitama 338-0012, Japan

(Received 29 November 1999; published 7 April 2000)

The elastic $^{17}O(^{16}O,^{16}O)^{17}O$ $(5/2^+)$ and inelastic $^{17}O(^{16}O,^{16}O)^{17}O^*$ $(1/2^+)$ scatterings are studied with a coupled-reaction-channel three-body model for $E_{\text{c.m.}}$ below 40 MeV. Without any parameter fit, the results agree fairly well with experiment for various deep and shallow $^{16}O+^{16}O$ potentials. In regions where no experimental data are available, the theoretical cross sections are sensitive to the choice of $^{16}O+^{16}O$ potential. The comparison of calculations with exactly phase-equivalent deep and shallow $^{16}O+^{16}O$ potentials deduced from supersymmetric transformations shows that this sensitivity is not related to the presence or absence of Pauli forbidden states. Assuming charge symmetry, we also calculate cross sections for the elastic $^{17}F(^{16}O,^{16}O)^{17}F$ $(5/2^+)$ and inelastic $^{17}F(^{16}O,^{16}O)^{17}F^*$ $(1/2^+)$ scatterings. The elastic cross sections of both mirror collisions display a strong backward rise for $E_{\text{c.m.}}>20$ MeV. Below 10 MeV, the inelastic $^{16}O+^{17}F$ excitation functions are strongly enhanced by the long range of the ^{17}F first excited state.

PACS number(s): 25.70.Bc, 25.60.Bx, 24.10.Eq, 24.10.Ht

I. INTRODUCTION

In principle, the theoretical study of heavy-ion scattering is a very complex many-body problem since it should take into account all the nucleons constituting the colliding nuclei. However, this problem can be strongly simplified if some of the constituent nucleons are assumed to form nuclear *clusters*, the internal structure of which can be neglected in a wide energy range. This approximation is particularly good when the clusters are doubly magic nuclei, like the α and ^{16}O nuclei, since these nuclei are very stable and undergo small deformations. The theoretical description then reduces to a few-body problem, each cluster being considered as a pointlike particle. Within this model, *ab initio* calculations can then be performed, with the interactions between the clusters as the only input data.

One of the systems for which such a cluster model is expected to be very good is the collision between an ^{16}O and an ^{17}O nucleus. The internal structure of the ^{16}O nucleus is not taken into account, while the ^{17}O nucleus is described as an ^{16}O core plus a valence neutron. We are thus faced with a three-body problem (instead of a 33-nucleon one). Two of these bodies are identical ^{16}O clusters, hence requiring application of the Pauli principle for the total wave function. Such calculations have already been successfully performed in Ref. [1], with a coupled-channel formalism, for both the $^{16}O+^{17}O$ elastic scattering and the inelastic scattering to the first excited state of ^{17}O, which also has an $^{16}O+$neutron structure (see also Ref. [2]).

In the present paper, we first reexamine these results with a more recent version of the coupled-channel formalism, allowing excitation to unbound states [3,4]. This allows us to test the convergence of the preceding calculations by introducing an additional resonance channel. We then study the influence of the $^{16}O+^{16}O$ potential on the results of the calculation. Indeed, very different phenomenological optical potentials exist in the literature for the $^{16}O+^{16}O$ system [5–12]. Roughly speaking, all these potentials provide similar fits to the $^{16}O+^{16}O$ elastic experimental data; i.e., they are approximately equivalent *on shell* or approximately *phase equivalent*. However, they have rather different features: their imaginary parts may depend on the angular momentum [7,9] or be transparent [8], and their real parts have various form factors. A striking difference between these potentials is that the most recent ones [9–13] support nonphysical and physical bound states (*deep* potentials), while the older ones only support physical bound states (*shallow* potentials). The coexistence of these very different potential families, as well as their phase equivalence, has been explained with the aid of supersymmetric transformations [14]. Using these potential families in a three-body model, as done below, can in principle reveal differences between their *off-shell* properties. Indeed, even if the total energy is a conserved quantity, the energy distribution between the three bodies can vary during the collision. If such off-shell effects are strong enough, the present model can help to solve the long-standing ambiguity between $^{16}O+^{16}O$ potentials.

Since the $^{16}O+^{17}O$ calculations are in good agreement with experiment without any parameter fit, we then use the same model to predict elastic and inelastic cross sections for the mirror collision, namely, $^{16}O+^{17}F$. For this purpose, we assume charge symmetry between both collisions; i.e., we use the same nuclear interactions and simply modify the electrostatic potentials. No experimental data are available for the $^{16}O+^{17}F$ collision because the ^{17}F nucleus is radioactive ($T_{1/2}=64.5$ s) and hence rather difficult to handle experimentally. However, recent progress in radioactive-ion-beam techniques have made ^{17}F beams available [15,16], and the $^{16}O+^{17}F$ collision can be studied experimentally with present-day technology. Such measurements would provide a good test of nuclear charge symmetry in these mirror collisions [17,4]. We hope that the present theoretical calcu-

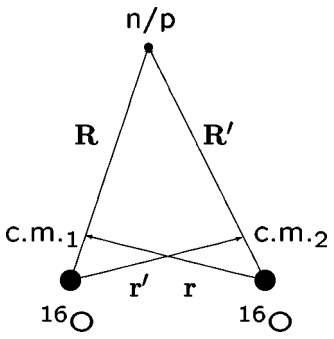

FIG. 1. Three-body model of the $^{16}O+^{17}O$ and $^{16}O+^{17}F$ systems: two ^{16}O cores and one valence nucleon. The center of mass of a core and the valence neutron is represented by c.m.$_i$ ($i=1,2$), but the proportions are modified for clarity.

lations will help to direct future experiments.

In Sec. II, we briefly describe the coupled-reaction-channel three-body model used to perform the calculations, as well as its necessary inputs, namely, the $^{16}O+$nucleon and $^{16}O+^{16}O$ interaction potentials. In Sec. III, we present the obtained excitation functions, both for the $^{16}O+^{17}O$ collision with a comparison to experimental results and for the $^{16}O+^{17}F$ mirror collision. Our conclusions and suggestions for new experiments are presented in Sec. IV.

II. MODEL

A. Coupled-reaction-channel three-body model

The $^{16}O+^{17}O$ and $^{16}O+^{17}F$ systems are both described in a three-body model, schematically represented in Fig. 1. We do not take the internal structure of the ^{16}O nucleus into account, while the ^{17}O and ^{17}F nuclei are described in a single-particle model, namely, an inert ^{16}O core in its 0^+ ground state interacting with a single nucleon. The coordinate between a first ^{16}O core and the valence nucleon is denoted by $\mathbf{R}$, while the relative coordinate between the two colliding nuclei is denoted by $\mathbf{r}$. The corresponding coordinates with respect to the other ^{16}O core are denoted with a prime. This allows us to write the total wave function in a compact form, which takes exactly into account the identity of the bosonic cores and thus the one-nucleon transfer reactions. The Hamiltonian of the system contains three potential terms: a core-core interaction and two identical core-nucleon interactions. These potentials are described in the next subsections.

In the present study, we limit ourselves to two-body channels of the $A+B$ form, where A is always an ^{16}O nucleus in its ground state, while B can be any state (bound or resonant) of the ^{17}O or ^{17}F nuclei with an $^{16}O+$nucleon structure. Other channels (involving either a core excitation or more than two bodies) are taken into account through a phenomenological optical (i.e., complex) core-core potential. In the calculations considered below, only the ground and first-excited bound states of the ^{17}O and ^{17}F nuclei will be used. A third resonant state will also be taken into account for a convergence test. The quantum numbers and energies of these three states are displayed in Table I.

TABLE I. Properties of the ^{17}O and ^{17}F bound and resonance states used in the calculation: total-angular-momentum quantum number I, parity π, energy E_i with respect to the $^{16}O+$nucleon system, resonance width Γ, and relative orbital momentum L in an $^{16}O+$nucleon model.

		^{17}O		^{17}F	
I^π	L	E_i (MeV)	Γ (MeV)	E_i (MeV)	Γ (MeV)
$\frac{5}{2}^+$	2	−4.144	-	−0.601	-
$\frac{1}{2}^+$	0	−3.273	-	−0.106	-
$\frac{3}{2}^+$	2	0.941	0.096	4.4	1.5

Remembering that an inert ^{16}O core has a zero spin and a positive parity, the channel wave functions of the three-body system are given by

$$\Phi_c^{JM\Pi}(\hat{\mathbf{r}},\mathbf{R})=[Y_l(\hat{\mathbf{r}})\otimes\phi_{E_iI\pi}(\mathbf{R})]^{JM}. \tag{1}$$

In this equation, J and M are the total-angular-momentum quantum numbers and Π is the total parity; these three numbers are good quantum numbers. The subscript c denotes the set of channel quantum numbers E_i, I, π, and l necessary to specify the particular channel. The quantum numbers E_i, I, and π are the energy, total angular momentum, and parity of the ^{17}O or ^{17}F nucleus, as given in Table I; $\phi_{E_iI\pi}(\mathbf{R})$ is a single-particle wave function describing the relative motion of the valence nucleon and the ^{16}O core, with an orbital momentum L. The quantum number l is the relative orbital momentum between the colliding nuclei, with $\hat{\mathbf{r}}$ the angular part of the corresponding coordinate.

For a given partial wave at energy E, the total wave function is a combination of channel wave functions multiplied by radial functions $u_c^{J\Pi}$:

$$\begin{aligned}\Psi^{JM\Pi}(\mathbf{r},\mathbf{R})&=\Psi^{JM\Pi}(\mathbf{r}',\mathbf{R}')\\&=\sum_{c=1}^{n}\left\{\Phi_c^{JM\Pi}(\hat{\mathbf{r}},\mathbf{R})\frac{u_c^{J\Pi}(r)}{r}\right.\\&\quad\left.+\Phi_c^{JM\Pi}(\hat{\mathbf{r}}',\mathbf{R}')\frac{u_c^{J\Pi}(r')}{r'}\right\}.\end{aligned} \tag{2}$$

This expression is symmetric with respect to core exchange, as required by the bosonic nature of the cores. All the ^{17}O and ^{17}F states considered in this article have a positive parity π (see Table I), which implies that the total parity Π of the system is $\Pi=\pi(-1)^l=(-1)^l$. For a given parity Π, all the l's must have the same parity. On the other hand, the angular momentum coupling imposes that, for a given total angular momentum J, l varies between $|J-I|$ and $J+I$. Taking into account these two conditions, the maximum number n of different channels entering Eq. (2) is 3, 4, or 6, depending on whether the lowest, the two lowest, or the three lowest states of Table I are considered in the calculation. Inserting expression (2) into the Schrödinger equation leads to a system of n coupled radial equations with an effective potential matrix; this system has to be solved at each energy to calculate

the radial wave functions $u_i^{J\Pi}(r)$. Within the *orthogonalized* coupled-reaction-channel method [3,4], the effective potential matrix can be made local by neglecting the recoil due to the transfer of the nucleon. This is a good approximation at low energies, even in cases where the no-recoil approximation is not good for calculations with the distorded-wave Born approximation or with the conventional coupled-reaction-channel method.

The diagonal part of the effective-interaction matrix is mainly due to the core + core (^{16}O+^{16}O) interaction which is discussed in detail below. The nondiagonal parts, i.e., the couplings between the different channels, are due to the presence of the valence nucleon. They are constructed from the core-nucleon and core-core interactions by folding them with the wave functions of the valence nucleon in the considered states. These wave functions are calculated in the single-nucleon shell model, with the core-nucleon potential described below.

B. ^{16}O+nucleon potential

Since we want to take advantage of the charge symmetry between both collisions, the nuclear part of this two-body potential should ideally be identical for both the ^{17}O and ^{17}F systems. We could not find such a potential in the literature. A parameter fit with a Woods-Saxon potential including a spin-orbit term is able to reproduce the bound and resonance states of Table I. Taking $\hbar/2\mu=22.032$ MeV fm^2 where μ is the reduced mass of the system, this potential reads

$$V(R)=\left(-56.7+V_{so}\mathbf{L}\cdot\mathbf{s}\frac{1}{R}\frac{d}{dR}\right)f(R,3.023,0.6415), \quad (3)$$

where energies are expressed in MeV and lengths in fm, and where $f(R,R_0,a)$ is the Woods-Saxon form factor with radius R_0 and diffuseness a:

$$f(R,R_0,a)=\left[1+\exp\left(\frac{R-R_0}{a}\right)\right]^{-1}. \quad (4)$$

The spin-orbit factor is, however, slightly different for both nuclei: $V_{so}=24.01$ MeV for ^{17}O and 25.14 MeV for ^{17}F. In the case of the ^{17}F nucleus, a Coulomb point-sphere potential is added to the above nuclear interaction. Its radius is the same as that of the Woods-Saxon potential: $R_C=3.023$ fm.

With these interactions, the single-particle states of Table I can be calculated by solving the two-body Schrödinger equation. The radial wave functions are shown in Fig. 2 for the ground and first-excited bound states of both the ^{17}O (solid lines) and ^{17}F (dashed lines) nuclei. Let us notice that the $s_{1/2}$ wave function has a node because of the occupied levels in the ^{16}O core. The comparison of the asymptotic behaviors of these wave functions is also interesting: for the ^{17}F nucleus, the range of the wave function is larger than for ^{17}O. The Coulomb repulsion of the ^{16}O+p system has two opposite effects on the single-particle wave functions, as compared with the ^{16}O+n system: on the one hand, the barrier effect reduces their range; on the other hand, the parameter of their exponential tail is decreased, which increases their range. For the $d_{5/2}$ state, these two effects roughly compensate each other, while for the $s_{1/2}$ state, the binding energy is so weak for ^{17}F that the exponential-tail effect is dominant. We shall see below that this has important consequences on the inelastic cross sections at low energy.

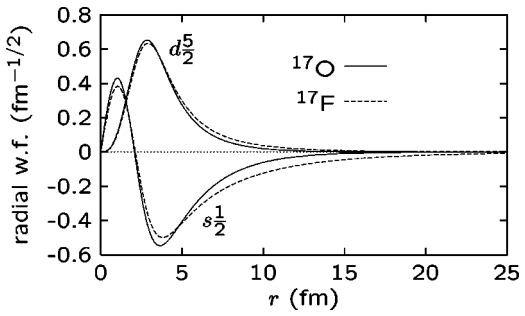

FIG. 2. Radial wave functions of the ground ($d_{5/2}$) and first excited ($s_{1/2}$) single-particle states for the ^{17}O (solid lines) and ^{17}F (dashed lines) nuclei. The nuclear interaction potential is that of Eq. (3), with an additional Coulomb potential in the ^{17}F case. The characteristics of these states are summarized in the first two lines of Table I.

C. Phenomenological ^{16}O+^{16}O potentials

A wide variety of such potentials exists. There are two main families: *shallow* potentials which only present physical bound states and *deep* potentials which in addition have nonphysical or forbidden bound states (FBSs) simulating the Pauli principle between the constituent nucleons [18–20]. For the ^{16}O+^{16}O system, microscopic models predict a number of Pauli forbidden states equal to

$$N=\frac{N_c-l_{^{16}O+^{16}O}}{2}, \quad (5)$$

where $l_{^{16}O+^{16}O}$ is the relative orbital momentum between the ^{16}O nuclei and $N_c=24$ is the so-called *critical* number [21]. Because of the identity of the colliding particles and of their bosonic character, only even partial waves have to be considered for the ^{16}O+^{16}O system. In the present calculation, the relative orbital momentum between the ^{16}O cores is not a good quantum number. However, we shall see below that some ^{16}O+^{16}O potentials depend on this number. Hence, we choose to approximate it by the relative orbital momentum between the colliding ^{16}O+^{17}O or ^{16}O+^{17}F nuclei:

$$l_{^{16}O+^{16}O}\approx l. \quad (6)$$

Both even and odd l's are thus used in the following. The number of forbidden states for odd-l partial waves is then chosen as the nearest integer above expression (5).

Shallow potentials were first successfully used to reproduce the experimental data in a satisfactory way, namely, the ^{16}O+^{16}O elastic cross sections and excitation functions [5–8]. They reproduce well the low-energy data (up to about 40 MeV c.m.), but fail to reproduce the higher-energy data [22]. Therefore, a deep potential with the right number of

TABLE II. Real part V and imaginary part W of the phenomenological $^{16}O+^{16}O$ potentials discussed in the text. The Woods-Saxon form factor $f(r,r_0,a)$ is defined in Eq. (4), E is the center-of-mass energy of the $^{16}O+^{16}O$ system in MeV, l is its relative orbital momentum, and r is the distance between both nuclei.

Potential	V (MeV)	W (MeV)
Chatwin [7]	$-17f(r,6.8,0.49)$	$\dfrac{-0.22E}{1+\exp\left(\dfrac{l-4.16\sqrt{E-6.7}}{0.4}\right)}f(r,6.8,0.49)$
Gobbi [8]	$-17f(r,6.8,0.49)$	$(-0.8-0.2E)f(r,6.4,0.15)$
Kondō [9]	$[-278.8+0.09l(l+1)]f(r,4.69,1.4)^2$	$\dfrac{-2.5-0.2E}{1+\exp(l-4.16\sqrt{E-8.5})}f(r,7,0.5)$

FBSs was proposed [9], which proved to be able to reproduce both the low- and high-energy data [10–13].

Below, we shall use three potentials which give a good description of the $^{16}O+^{16}O$ scattering data in the energy range 10 MeV $<E_{\mathrm{c.m.},^{16}O+^{16}O}<35$ MeV (just above the Coulomb barrier). The first two ones belong to the shallow family and were proposed in the early 1970s [7,8], while the last one is deep and was proposed in 1989 [9]. Their parameters are listed in Table II. For the coupled-channel calculations, the relative energy between the ^{16}O cores is approximated by the relative energy between the colliding nuclei:

$$E_{^{16}O+^{16}O}\approx E. \tag{7}$$

Thanks to approximations (6) and (7), the subscript "$^{16}O+^{16}O$" will not be used any more in the following.

1. Chatwin potential

Proposed in Ref. [7], this potential has the same real part as that constructed in Ref. [6], but a more complicated imaginary part which allows a better reproduction of the data. It has a Woods-Saxon form factor for both the real and imaginary parts. It has a shallow real part with all parameters independent of energy and angular momentum. Its imaginary part is more complicated: its depth depends linearly on energy, but it is also multiplied by a smooth cutoff factor which vanishes when the angular momentum is larger than a critical value. This critical value separates the strongly absorbed partial waves (low angular momenta) from the weakly absorbed ones (high angular momenta); it thus depends on energy, as shown in Table II.

2. Gobbi potential

This potential, proposed in Ref. [8], aims at providing the same quality of fit to experiment as the preceding one, but with a simplified form. The real part is exactly the same as that of the preceding potential, as seen in Table II. The imaginary part is simpler but its radius is shorter than that of the real part, which means that this potential is surface transparent. The complicated orbital momentum dependence is not necessary to reproduce experimental data. The depth of the imaginary part simply increases linearly with energy, which aims at reproducing the opening of channels with increasing energy.

3. Kondō potential

This potential is one among those proposed in Ref. [9] and is deep. Its number of Pauli forbidden states, which depends on the relative orbital momentum, is given by Eq. (5). Moreover, in comparison with the above shallow potentials, it has one additional bound state in partial waves $l=0-24$; these bound states are interpreted as molecular highly excited states of ^{32}S with an $^{16}O+^{16}O$ molecular structure, but no experimental evidence exists for them. As quoted in Ref. [9], deep potentials without such "physical states" can also be found, but according to Refs. [10,11], a deep potential valid at higher energies should have two such "physical states" in partial waves $l=0-24$ and one in partial wave $l=26$.

The Kondō potential has a slight l dependence in its real part. The imaginary part of the potential has the same complicated form as that of the Chatwin potential, but the parameters are different, as can be seen in Table II. Deep potentials with a Gobbi-type imaginary part do not seem to allow a good reproduction of the experimental data [23].

D. Phase-equivalent $^{16}O+^{16}O$ potentials

The phenomenological potentials just described are not exactly phase equivalent. Actually, they only provide *similar* fits to experimental cross sections, which means that their phase shifts are only roughly similar. One of the aims of this work is a comparison of the off-shell properties of deep and shallow potentials which are *exactly* equivalent on shell. Such exactly phase-equivalent $^{16}O+^{16}O$ potentials have been constructed in Ref. [14]. Let us summarize these results here.

The simplest way to construct phase-equivalent potentials is to remove the forbidden bound states from a deep potential, which leads to a shallow potential. Phase equivalence can be guaranteed throughout this removal with pairs of supersymmetric transformations [24]: the first transformation removes the bound state but modifies the phase shift; afterwards the second transformation does not modify the bound spectrum anymore but restores the phase shift.

This method has been generalized to complex (optical) potentials in Ref. [25] and applied to the $^{16}O+^{16}O$ case in Ref. [14]. The formula relating an initial effective potential

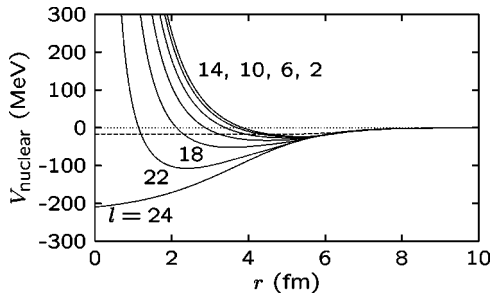

FIG. 3. Nuclear real part of the $^{16}O+^{16}O$ effective potentials constructed by supersymmetric phase-equivalent removal [Eq. (8)] of N [Eq. (5) with $N_c=24$] Pauli forbidden states from the deep potential of Ref. [9], for partial waves $l=24,22,18,14,\ldots,2$ (solid lines). The shallow potential of Refs. [6–8] is represented by a dashed line for comparison.

V_0 with a phase-equivalent potential V_2 with one bound state fewer reads

$$V_2(r)=V_0(r)-2\frac{d}{dr}\left(\frac{\psi_0(E_0,r)^2}{\int_0^r \psi_0(E_0,t)^2 dt}\right), \qquad (8)$$

where ψ_0 is the normalized (complex) wave function of the removed normalizable state at the (complex) energy E_0.

For each partial wave, all the forbidden bound states of a given deep potential can be removed by iterating Eq. (8), which leads to an exactly phase-equivalent shallow potential. In Ref. [14], this procedure is applied to the deep Kondo potential. The transformation does nearly not modify the imaginary part of the potential. On the contrary, its real part is strongly affected: it becomes shallower and gets an r^{-2} repulsive core at the origin. The real part of the obtained potentials without Coulomb or centrifugal terms is shown in Fig. 3 for partial waves $l=24,22,18,14,\ldots,2$ (solid lines). According to Eq. (5) with $N_c=24$, only partial waves with $l<24$ possess forbidden bound states which can be removed. The number of removed states depends on l, which explains the strong l dependence of the potential shown in Fig. 3. For $l\geqslant 24$, no bound-state removal is performed and the effective potential, although it has no forbidden bound state, is deep in the sense that its purely nuclear part is deep. For lower partial waves, forbidden bound states are removed and the nuclear part of the obtained potentials becomes shallower. It is also shown in Fig. 3 that, while the Kondo potential is very different from the shallow potential of Refs. [6–8] (dashed line) below 6 fm, its supersymmetric partners for the lowest partial waves are close to that potential down to about 4 fm (the differences below 4 fm are less significant since absorption is strong there [8]). In Ref. [14], both potentials are even made closer to one another by removing a number of bound states (5) with $N_c=26$ instead of 24. This allows the removal of the molecular states mentioned above (which have no equivalent in the shallow phenomenological potentials) in addition to the removal of the Pauli forbidden states.

In conclusion, supersymmetry establishes a connection between the deep and shallow families of potentials for low partial waves. This implies that elastic scattering data at low energies, i.e., energies for which partial waves with $l<24$ are predominant, do not allow solving the long-standing ambiguity problem between deep and shallow potentials. On the contrary, for higher partial waves ($l\geqslant 24$), the difference between deep and shallow phenomenological potentials cannot be explained by the presence of FBSs, which means that scattering data at energies where some of these partial waves are dominant can solve the ambiguity. This is indeed the case: only deep potentials can explain the high-energy data. In the following, we shall consider an energy region where the dominant partial waves are below $l=24$, i.e., where *a priori* both potential families can be used, and we shall compare their off-shell properties.

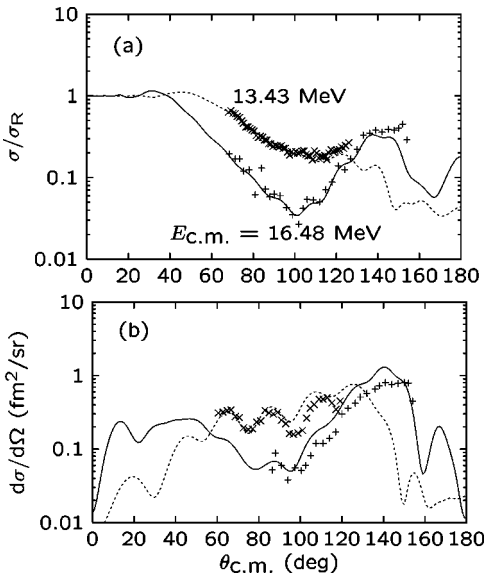

FIG. 4. Elastic (a) and inelastic (b) angular distributions of the $^{16}O+^{17}O$ differential cross sections at $E_{\text{c.m.}}=13.43$ MeV (dashed lines, diagonal crosses) and 16.48 MeV (solid lines, vertical crosses). The theoretical curves are obtained with two-channel calculations using the Chatwin core-core potential. The experimental data come from Refs. [26] (16.48 MeV, elastic), [27] (16.48 MeV, inelastic), and [28] (13.43 MeV).

III. RESULTS

A. $^{16}O+^{17}O$ collision

As known for 25 years [1], the present three-body model provides a very satisfactory description of this collision, due to the closed-shell structure of the ^{16}O core. In Fig. 4, for instance, we compare the elastic (a) and inelastic (b) theoretical cross sections at $E_{\text{c.m.}}=13.43$ and 16.48 MeV with experimental data from Refs. [26–28]. The agreement is satisfactory and we have verified that it is also the case at other energies where experimental angular distributions are available, namely, $E_{\text{c.m.}}=11.33$, 12.36, 14.42, and 15.51 MeV. Let us insist on the fact that this agreement is obtained without any fit (except for a normalization of the yields of Ref. [28]), which implies that the present method has a predictive power. This is important for the mirror reaction considered below, for which no experimental data are available.

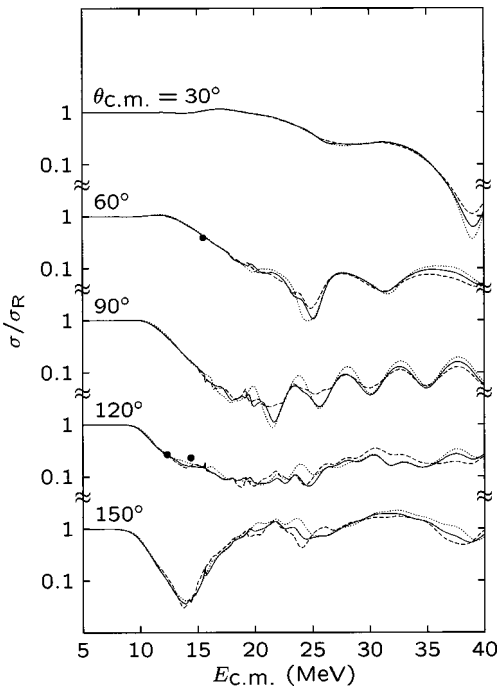

FIG. 5. One- (dotted lines), two- (solid lines), and three- (dashed lines) channel calculations of the elastic excitation functions of the $^{16}O+^{17}O$ collision at $\theta_{c.m.}=30°$, 60°, 90°, 120°, and 150°, with the Chatwin core-core potential. Experimental data are extracted from angular distributions of Refs. [26,28] and σ_R is the Rutherford cross section.

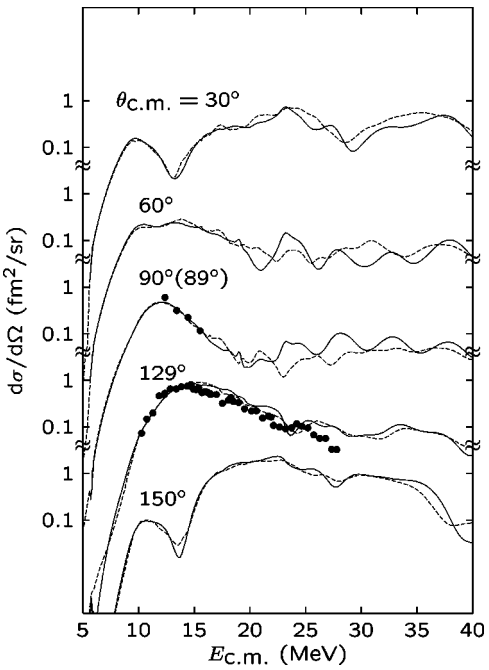

FIG. 6. Same as Fig. 5, but for the inelastic excitation functions at 30°, 60°, 90°, 129°, and 150°. Experimental data at 129° as well as four experimental points at 89°, coming from Refs. [27,28], are also shown.

In the following, we shall see that the cross sections have interesting features in a wider energy region than the one covered experimentally, and we choose to show excitation functions rather than angular distributions. In Fig. 5, five different elastic excitation functions between 5 and 40 MeV are drawn; they are calculated with one (dotted lines), two (solid lines), and three (dashed lines) channels, corresponding to the ^{17}O states described in Table I. In Fig. 6, we show the corresponding inelastic excitation functions obtained by the two- and three-channel calculations. The agreement with experimental data from Refs. [26–28] is good (at $\theta_{c.m.}=129°$, the inelastic excitation function has been measured, while the other points are extracted from angular distributions).

The three-channel calculation results from a generalization to resonance states of the orthogonalized coupled-reaction-channel method [3], as presented in Ref. [4]. It allows us to test the intrinsic convergence of our calculation by comparing this result to the one- and two-channel calculations. Figures 5 and 6 show that the inclusion of the third channel does not qualitatively affect the results. Its effect is the most important in the 60° and 90° inelastic excitation functions above 20 MeV. In these figures, we have used the Chatwin core-core potential; we have verified that the same conclusions hold for the other core-core potentials considered below. We can thus conclude that the convergence of our calculation is good, and in the following we shall limit ourselves to two-channel calculations.

This result contrasts to that obtained in the calculation of the $^{12}C+^{13}C$ and $^{12}C+^{13}N$ scattering systems [4], where the $d_{3/2}$ channel greatly affects the coupled-reaction-channel scheme of the total system. This difference is reasonably explained by the fact that the $p_{1/2}$ state is accessible to the valence nucleon in the ^{13}C and ^{13}N nuclei, while it is not in the ^{17}O and ^{17}F nuclei. In the $^{12}C+^{13}C$ and $^{12}C+^{13}N$ systems, the approaching ^{12}C nucleus may thus induce a mixing of the $p_{1/2}$ and $d_{3/2}$ states in the ^{13}C and ^{13}N nuclei. Such a different-parity mixing, also described as a ''hybridization'' phenomenon, causes strong coupled-reaction-channel effects, in analogy to the strong binding phenomena due to the mixing of sp orbitals of electrons in covalent molecules. In the $^{16}O+^{17}O$ and $^{16}O+^{17}F$ systems, such a hybridization phenomenon cannot be expected since all states accessible to the valence nucleon have the same parity.

B. Influence of the $^{16}O+^{16}O$ potential

Let us now test the dependence of the previous results on the choice of phenomenological core-core potential. In Figs. 7 and 8, the same excitation functions as in Figs. 5 and 6 are calculated with the three different potentials presented above: the Chatwin potential (solid lines), the Gobbi potential (dotted lines), which has the same real part as the preceding one but a different imaginary part, and the Kondo potential (dashed lines), which also has a very different real part (see discussion above and Table II). Although these potentials lead to qualitatively different results, the experimental data are insufficient to dismiss any of them. In the descent just above the Coulomb barrier, the elastic cross sections obtained with the Kondo potential are slightly smaller than those obtained with the shallow potentials. This can be related to the fact that the Coulomb barrier is about 0.7 MeV

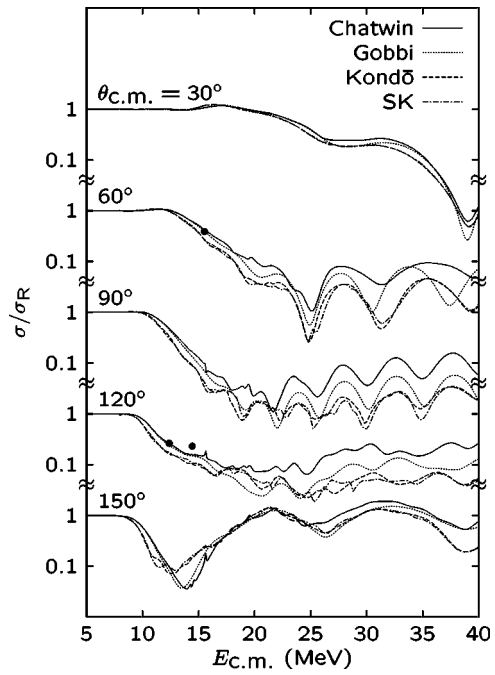

FIG. 7. Comparison of the elastic excitation functions with two-channel calculations using the Chatwin (solid lines), Gobbi (dotted lines), and Kondō (dashed lines) phenomenological potentials, as well as the supersymmetric partner of the Kondō potential (SK, dash-dotted lines) presented in Fig. 3.

smaller for the Kondō potential than for the Chatwin and Gobbi potentials (a similar effect is observed in the $^{16}O+^{16}O$ elastic excitation functions). At higher energies and for angles between 60° and 120°, more significant differences occur in both the elastic and inelastic cross sections: the Chatwin cross sections are larger than the Gobbi cross sections, which are larger than the Kondō cross sections. Since these differences sometimes reach one order of magnitude, new experimental results in these region should allow discriminating between the core-core potentials. Let us, however, notice that these differences occur in regions where the absolute magnitude of the cross section is small. In regions where the cross section is large, the agreement between the different models is much better. For instance, let us point out the high value of the elastic excitation function at 150° above 20 MeV, as shown in Fig. 7. It implies a strong backward rise in the elastic cross sections at these energies, which is due to the elastic transfer of the valence nucleon. A similar enhancement is also seen in the inelastic excitation function at the same angle and in the same energy region.

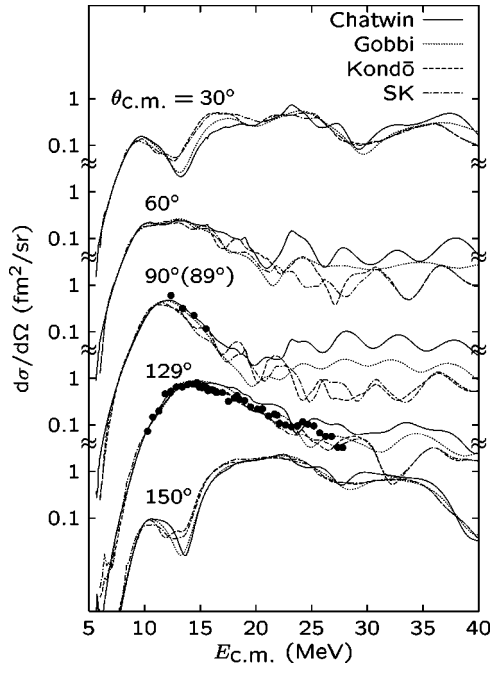

FIG. 8. Same as Fig. 7 but for the inelastic excitation functions.

Since both the Chatwin and Gobbi potentials have the same real part, Figs. 7 and 8 allow us to see how strong the influence of the imaginary part of the core-core potential is on the three-body calculation. With the transparent Gobbi potential, the absorption is more important since both the elastic and inelastic cross sections are reduced at intermediate angles. In general, the switch from the shallow Chatwin potential to the deep Kondō one decreases the elastic and inelastic excitation functions even more, which suggests that the modification of the real part of the core-core potential also has an effect. This seems to indicate that the deep or shallow character of this potential influences the present results. To check this, we perform the same calculations with the supersymmetric shallow partner of the Kondō potential presented above. In Figs. 7 and 8, the curves obtained with this potential (dash-dotted lines) are very similar to the ones obtained with the original Kondō potential. We conclude that the presence or absence of forbidden states has no influence on the three-body calculations; the difference between the Chatwin and Kondō calculations is thus due to (i) the modification of the imaginary part and (ii) slight on-shell differences between both potentials (for instance, between the heights of their Coulomb barriers).

The above results show either that deep and shallow potentials, which are exactly phase equivalent on shell, also have very similar properties off shell, or that the $^{16}O+^{17}O$ collision slightly depends on off-shell effects of the core-core interaction. It is shown in Ref. [8] that for the $^{16}O+^{16}O$ collision, the partial waves with $l \geqslant 24$ do not play a significant role below 40 MeV; we have verified that it is also the case for the $^{16}O+^{17}O$ collision. Consequently, we can conjecture that, as for the $^{16}O+^{16}O$ collision, the difference between deep and shallow potentials, which cannot be avoided for $l \geqslant 24$ (see Fig. 3), would probably have consequences at higher energies, where these partial waves play a dominant role. There, only deep potentials would be satisfactory. We have not checked this point here since at those energies the recoil effects should be taken into account, which complicates the calculations.

C. $^{16}O+^{17}F$ mirror collision

Let us now take advantage of the charge symmetry of the nuclear interaction to predict cross sections for this reaction. In Fig. 9, using a two-channel calculation with the Chatwin

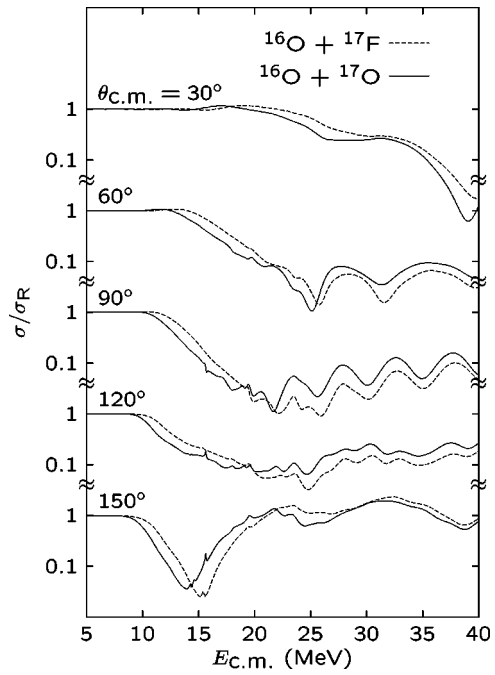

FIG. 9. Comparison of the $^{16}O+{}^{17}O$ (solid lines) and $^{16}O+{}^{17}F$ (dashed lines) elastic excitation functions, using a two-channel calculation with the Chatwin core-core potential.

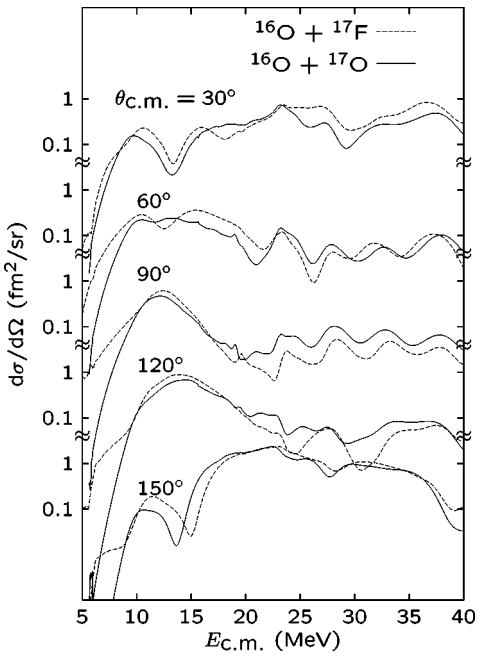

FIG. 10. Same as Fig. 9 but for the inelastic excitation functions.

core-core potential, the elastic excitation functions of both reactions are compared. They display the same qualitative behavior, with, however, an energy shift of about 1 MeV. This can be explained by the higher Coulomb barrier for the $^{16}O+{}^{17}F$ system than for the $^{16}O+{}^{17}O$ system. We have checked that the influence of the core-core potential on the $^{16}O+{}^{17}F$ scattering is similar to its influence on the $^{16}O+{}^{17}O$ case. Hence, the uncertainty in the predictions is rather big at angles near 90° where the direct and transfer scattering amplitudes strongly interfere with each other and where the cross sections are small. Let us, however, insist on the fact that some important features of the excitation functions, like the strong backward rise in the elastic cross section at energies above 20 MeV, are independent of the choice of the core-core potential.

Figure 10 compares the inelastic excitation functions of both reactions. They are also close to one another, with the important exception of the low-energy ($E_{c.m.}<10$ MeV) results at large angles ($\theta_{c.m.}>90°$). There the $^{16}O+{}^{17}F$ cross section is strongly enhanced. This has to be put in connection with the large spatial extension of the ^{17}F first excited state (see Fig. 2) which increases the coupling between the channels. The same effect is seen on the angle-integrated inelastic cross section shown in panel (a) of Fig. 11: below 8 MeV, the ^{17}F cross section (dashed line) is much larger than the ^{17}O one (solid line). The ^{17}O curve is in good agreement with the experimental results of Ref. [29]. For comparison, the fusion cross section, obtained from the matrix elements of the non-Hermitian part of the effective potential matrix [4], is also shown in panel (b). There both curves display the same behavior with a 1-MeV difference due to the difference of Coulomb barrier. The agreement between the ^{17}O theoretical curve and the experimental data of Ref. [29] is not as good as for the inelastic cross sections, but remains satisfactory for an *ab initio* calculation. The enhancement effect of the inelastic cross section is so strong that it also appears in the reaction cross section [panel (c)], which is approximated

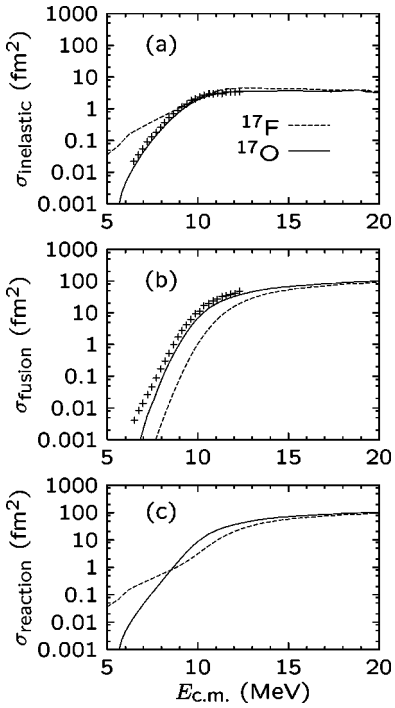

FIG. 11. Angle-integrated inelastic (a), fusion (b), and reaction (c) cross sections of the $^{16}O+{}^{17}O$ (solid lines) and $^{16}O+{}^{17}F$ (dashed lines) collisions, obtained with a two-channel calculation with the Chatwin potential. The reaction cross section is here the sum of the inelastic and fusion ones. Experimental results for the $^{16}O+{}^{17}O$ case come from Ref. [29].

here by summing the inelastic and fusion cross sections of panels (a) and (b).

IV. CONCLUSIONS

We have used a three-body coupled-channel model to calculate the elastic excitation functions of the $^{16}O+^{17}O$ and $^{16}O+^{17}F$ mirror collisions, as well as the inelastic excitation function to the first excited state of ^{17}O and ^{17}F. In this model, the ^{17}O and ^{17}F nuclei are described by an inert ^{16}O cluster and a valence nucleon. With the core-core and core-nucleon two-body interactions as only input, the model agrees with the available experimental data for the $^{16}O+^{17}O$ collision, without any parameter fit. The convergence of the model has been tested by introducing a third channel corresponding to a resonance state of the ^{17}O and ^{17}F nuclei.

The calculation is sensitive to the $^{16}O+^{16}O$ interaction, mainly at intermediate angles for $E_{\text{c.m.}}>20$ MeV (see Figs. 7 and 8). Available experimental data in this region are not sufficient to dismiss any of the tested core-core interactions, and new experimental results would be useful. Various phenomenological $^{16}O+^{16}O$ potentials have been used, which reveal that both their real and imaginary parts have an influence on the excitation functions. However, since these potentials are not exactly equivalent on shell, this influence cannot be unambiguously attributed to off-shell effects. We have also tested that, contrary to what could be expected, the deep or shallow character of the $^{16}O+^{16}O$ interaction does nearly not influence the result below 40 MeV. Indeed, two calculations performed with exactly phase-equivalent supersymmetric partners lead to very close results, and no off-shell effects could be clearly seen either. We conjecture that for the present systems as for the $^{16}O+^{16}O$ one, only higher-energy results should be more favorable to deep potentials than to shallow potentials.

Using charge symmetry (identical nuclear interactions for both mirror systems), we have predicted elastic and inelastic excitation functions of the $^{16}O+^{17}F$ collision. This collision has not been measured up to now because of the difficulty of handling the radioactive ^{17}F nucleus. Thanks to the progress of radioactive-ion-beam techniques, ^{17}F beams are now available [15,16]. The present calculation shows the interest of measuring both the $^{16}O+^{17}O$ and $^{16}O+^{17}F$ collisions. At center-of-mass energies below 10 MeV, the inelastic $^{16}O+^{17}F$ collision displays a strong enhancement due to the long-range tail of the ^{17}F first-excited-state wave function. At energies above 20 MeV, both the elastic and inelastic cross sections are very large at backward angles. Finally, the comparison of experimental results with our calculations would allow a test of charge symmetry for these mirror reactions [17].

ACKNOWLEDGMENTS

J.-M.S. is supported by the National Fund for Scientific Research, Belgium. This text presents research results of the Belgian program P4/18 on interuniversity attraction poles initiated by the Belgian-state Federal Services for Scientific, Technical and Cultural Affairs.

[1] B. Imanishi, H. Onishi, and O. Tanimura, Phys. Lett. **57B**, 309 (1975).
[2] G. Baur and H. H. Wolter, Phys. Lett. **51B**, 205 (1974).
[3] B. Imanishi and W. von Oertzen, Phys. Rep. **155**, 29 (1987).
[4] B. Imanishi, V. Denisov, and T. Motobayashi, Phys. Rev. C **55**, 1946 (1997).
[5] R. H. Siemssen, J. V. Maher, A. Weidinger, and D. A. Bromley, Phys. Rev. Lett. **19**, 369 (1967).
[6] J. V. Maher, M. W. Sachs, R. H. Siemssen, A. Weidinger, and D. A. Bromley, Phys. Rev. **188**, 1665 (1969).
[7] R. A. Chatwin, J. S. Eck, D. Robson, and A. Richter, Phys. Rev. C **1**, 795 (1970).
[8] A. Gobbi, R. Wieland, L. Chua, D. Shapira, and D. A. Bromley, Phys. Rev. C **7**, 30 (1973).
[9] Y. Kondō, B. A. Robson, and R. Smith, Phys. Lett. B **227**, 310 (1989).
[10] Y. Kondō, F. Michel, and G. Reidemeister, Phys. Lett. B **242**, 340 (1990).
[11] Y. Sugiyama, Y. Tomita, H. Ikezoe, Y. Yamanouchi, K. Ideno, S. Hamada, T. Sugimitsu, M. Hijiya, and Y. Kondō, Phys. Lett. B **312**, 35 (1993).
[12] Y. Kondō, Y. Sugiyama, Y. Tomita, Y. Yamanouchi, H. Ikezoe, K. Ideno, S. Hamada, T. Sugimitsu, M. Hijiya, and H. Fujita, Phys. Lett. B **365**, 17 (1996).
[13] M. P. Nicoli, F. Haas, R. M. Freeman, N. Aissaoui, C. Beck, A. Elanique, R. Nouicer, A. Morsad, S. Szilner, Z. Basrak, M. E. Brandan, and G. R. Satchler, Phys. Rev. C **60**, 064608 (1999).
[14] J.-M. Sparenberg and D. Baye, Phys. Rev. C **54**, 1309 (1996).
[15] B. Harss *et al.*, Phys. Rev. Lett. **82**, 3964 (1999).
[16] D. W. Bardayan *et al.*, Phys. Rev. Lett. **83**, 45 (1999).
[17] E. Liénard, D. Baye, T. Delbar, P. Descouvemont, P. Duhamel, W. Galster, M. Kurokawa, P. Leleux, I. Licot, P. Lipnik, C. Michotte, T. Motobayashi, A. Ninane, J. Vanhorenbeeck, and J. Vervier, Phys. Rev. C **52**, 775 (1995).
[18] V. I. Kukulin, V. G. Neudatchin, and Y. F. Smirnov, Nucl. Phys. **A245**, 429 (1975).
[19] B. Buck, H. Friedrich, and C. Wheatley, Nucl. Phys. **A275**, 246 (1977).
[20] H. Horiuchi, in *Trends in Theoretical Physics*, edited by P. J. Ellis and Y. C. Tang (Addison-Wesley, Harlow, U.K., 1991), Vol. 2, Chap. 13, pp. 277–349.
[21] D. Baye and G. Reidemeister, Nucl. Phys. **A258**, 157 (1976).
[22] M. L. Halbert, C. B. Fulmer, S. Raman, M. J. Saltmarsh, A. H. Snell, and P. H. Stelson, Phys. Lett. **51B**, 341 (1974).
[23] Y. Kondō (private communication).
[24] D. Baye, Phys. Rev. Lett. **58**, 2738 (1987).
[25] D. Baye, G. Lévai, and J.-M. Sparenberg, Nucl. Phys. **A599**, 435 (1996).
[26] C. K. Gelbke, R. Bock, P. Braun-Munzinger, D. Fick, K. D.

Hildenbrand, W. Weiss, S. Wenneis, and G. Baur, Phys. Lett. **43B**, 284 (1973).

[27] C. K. Gelbke, G. Baur, R. Bock, P. Braun-Munzinger, W. Grochulski, H. L. Harney, and R. Stock, Nucl. Phys. **A219**, 253 (1974).

[28] D. Kalinsky, D. Melnik, U. Smilansky, N. Trautner, B. A. Watson, Y. Horowitz, S. Mordechai, G. Baur, and D. Pelte, Nucl. Phys. **A250**, 364 (1975).

[29] J. Thomas, Y. T. Chen, S. Hinds, D. Meredith, and M. Olson, Phys. Rev. C **33**, 1679 (1986).